RSC Advances

PAPER

View Article Online
View Journal | View Issue

Cite this: *RSC Adv.*, 2022, **12**, 6409

Comparative investigation of bioflavonoid electrocatalysis in 1D, 2D, and 3D carbon nanomaterials for simultaneous detection of naringin and hesperidin in fruits†

Hong-qi Xia,[a] Tingting Gu,[b] Ruiyi Fan[a] and Jiwu Zeng *[a]

Electrocatalysis of bioflavonoids in carbon nanomaterials plays an important role in electrochemical sensors for the detection of their content in fruits. In this study, three types of carbon nanomaterials with 1D, 2D, and 3D structures, namely carbon nanotubes (CNTs), graphene oxide (GO), and Ketjen black (KB), were modified onto glassy carbon electrodes for the electrocatalysis of hesperidin and naringin, which are two important bioflavonoids in fruits. As a result, the CNT-modified electrodes showed the highest electrocatalytic activity for both hesperidin and naringin compared to GO and KB. The morphology and surface chemistry of the carbon nanomaterials were characterized. The structural defects and carbon status of carbon nanomaterials are proposed to be the most important factors affecting the electrocatalysis of hesperidin and naringin. Finally, a CNT-based electrochemical sensor was fabricated to simultaneously detect hesperidin and naringin. Real sample tests on the fruit extract of *Citrus grandis* "Tomentosa" show that the proposed electrochemical sensors with high recovery thus could be employed in practical applications.

Received 28th September 2021
Accepted 13th February 2022

DOI: 10.1039/d1ra07217j

rsc.li/rsc-advances

Introduction

Bioflavonoids, a group of polyphenolic compounds widely distributed in plants, have attracted increasing attention in the past few decades owing to their health-promoting effects, such as anti-oxidant, anti-aging, anti-cancer, anti-neurodegenerative, and photoprotective properties.[1–3] For example, several researchers have demonstrated that naringin, an important citrus flavoglycoside, protects the mouse liver and intestine against radiation-induced damage by elevating the antioxidant status and reducing lipid peroxidation.[4] Furthermore, hesperidin, a citrus flavanone glycoside composed of hesperedin (an aglycone unit) and rutinose (a disaccharide), has been reported to play an important role in COVID-19 prevention.[5,6] The content of bioflavonoids varies in different plants, and even in different parts or different life cycle phases of the same plant.[7] Therefore, rapid, simple, and reliable detection of bioflavonoids in such agricultural products is essential for daily food control, orchard management, and metabolomic studies. Separation-based analytical methods, such as high-performance liquid chromatography[8] and gas chromatograph,[9] are conventionally used for bioflavonoid determination with high sensitivity; however, they require complex and expensive equipment operated by professional technicians.

Bioflavonoids are recognized as antioxidants because of their ability to scavenge radicals by electron transfer processes.[10] From this viewpoint, electrocatalysis involving interfacial electron transfer at electrodes can be employed for rapid bioflavonoid determination.[11] Indeed, several studies on the electrochemical detection of bioflavonoids have been reported, especially using electrodes functionalized with different nanomaterials, such as gold nanocage,[12] gold nanoparticles,[13] carbon nanotubes,[14] graphene oxides,[15] carbon nanoparticles[16] and their combinations.[17–20] For example, Sebastian *et al.* reported a amine-functionalized multi-walled carbon nanotube (CNT) and 3D rose flower-like zinc oxide nanocomposite for electrochemical detection of morin.[19] Gao *et al.* developed gold nanoparticles and reduced graphene oxide hybrid electrodes for hesperidin detection.[20] However, the role of such nanomaterials in the electrooxidation of bioflavonoids remains unclear. Furthermore, the comparison of bioflavonoid electrocatalysis at different carbon nanomaterials, among the most widely utilized nanomaterials owing to their low cost and affordable industrial scalability, has not yet been investigated systemically.

In this study, three types of carbon nanomaterials, namely carbon nanotubes CNTs, GO, and Ketjen black (KB), were investigated for the electrocatalysis of naringin and hesperidin, two of the most important bioflavonoids in fruits. CNTs are one-

[a]*Key Laboratory of South Subtropical Fruit Biology and Genetic Resource Utilization (MARA), Guangdong Province Key Laboratory of Tropical and Subtropical Fruit Tree Research, Institute of Fruit Tree Research, Guangdong Academy of Agricultural Sciences, Guangzhou 510640, China. E-mail: jiwuzeng@163.com*

[b]*School of Chemical Engineering, University of Science and Technology Liaoning, Anshan 114051, China*

† Electronic supplementary information (ESI) available. See DOI: 10.1039/d1ra07217j

dimensional (1D) carbon nanowires consisting of one or more layers of seamlessly rolled graphene (single-walled and multi-walled CNTs).[21] GO, the oxidized form of graphene, are two-dimensional (2D) carbon nanosheets with abundant oxygen-containing functional groups.[22] KB, a carbon nanoparticle material with three-dimensional (3D) mesoporous structure, is frequently utilized as a catalyst support in electrocatalytic reactions.[23] All three types of carbon nanomaterials with nanoscale structures, excellent electrical conductivities, and large specific surface areas (in a precise sense, with large surface-to-weight ratios) have been widely utilized in electrochemical and electroanalytical fields for different purposes, for example as electrode materials for enzyme immobilization in bioelectrocatalysis.[24–26] Furthermore, such carbon nanomaterials have also been employed directly as metal-free catalysts for various electrocatalysts, including oxygen reduction, water oxidation, and glucose oxidation.[27,28] However, the performance of such electrocatalysts varies depending on the carbon nanomaterial selected.[29,30]

Herein, the electrocatalysis of bioflavonoids in the selected 1D, 2D, and 3D carbon nanomaterials were investigated and compared. The morphology and surface chemistry of the three types of carbon nanomaterial-modified electrodes were investigated and compared by scanning electron microscopy (SEM), X-ray power diffraction (XRD), X-ray photoelectron spectroscopy (XPS), and Raman spectroscopy. The effects of the characteristics of carbon nanomaterials on the electrocatalysis of bioflavonoids were analyzed and discussed. Kinetic analysis was carried out to explore the mechanism of the electrooxidation of naringin and hesperidin. Consequently, electrochemical sensors for the simultaneous detection of naringin and hesperidin were designed and fabricated. Real sample tests on the fruits extract of *Citrus grandis* "Tomentosa" (CGT), a famous citrus cultivar that has been employed as a cough suppressant and expectorant in traditional Chinese medicine for thousands of years,[31] show that the proposed electrochemical sensors exhibit high sensitivity, selectivity, and recovery and could be employed for the detection of bioflavonoids in fruits.

Experimental

Materials and chemicals

Multi-walled CNTs (NC7000) with an average diameter of 9.5 nm, average length of 1.5 μm, and purity of 90% were obtained from Nanocyl S.A., GO with a purity greater than 99% was obtained from MACKLIN reagent Co. China, Ketjen black EC300J was obtained from Lion Co. Japan. Hesperidin, naringin, and Nafion 117 solution were purchased from Aladdin biochemical co. China. All other chemicals used in this study were of analytical grade, and all solutions were prepared with distilled water unless otherwise specified.

Preparation of carbon nanomaterials modified electrodes

Glassy carbon (GC) electrodes were polished with alumina slurry, sonicated, and washed with distilled water. Carbon nanomaterials were dispersed in ethanol containing Nafion 117 by sonication for 1 h. Carbon nanomaterial slurry (2.5 μL) was applied onto the GC electrode surface and dried at room temperature. This operation was repeated four times, and the final amount of carbon nanomaterial was approximately 30 μg. The prepared carbon-nanomaterial modified GC electrodes are referred to as CNT/Nafion/GC electrodes, GO/Nafion/GC electrodes, and KB/Nafion/GC electrodes, respectively.

Electrochemical measurements

All electrochemical experiments were performed on a CHI660E electrochemical analyzer (Chenhua, China) with a three-electrode system comprising a GC electrode (3 mm diameter) as the working electrode, Ag/AgCl (sat. KCl, CHI) reference electrode, and platinum wire auxiliary electrode (1 mm diameter). All potentials were measured with respect to the reference electrode in this study. A 0.2 M phosphate buffer (pH 7.0 ± 0.1) was used as the electrolyte solution.

Characterization

The morphology of the carbon nanomaterial-modified electrodes was characterized using SEM (Quanta 450, FEI). XRD patterns of the carbon nanomaterials were studied by an X-ray powder diffractometer (Empyrean), Raman spectra of the carbon nanomaterials were acquired by Raman spectroscopy (RENISHAW inVia), and XPS of the carbon nanomaterials was performed using an X-ray photoelectron spectrometer (ESCALAB Xi+, Thermo Fisher Scientific).

Results and discussion

Characteristics of the carbon-nanomaterials modified electrodes

Before the electrochemical measurements were performed, the surface morphologies of the carbon-nanomaterial modified GC electrodes were examined by SEM. As shown in Fig. 1A–C, rough surfaces with 3D structures were found on all carbon-nanomaterial modified GC electrodes, as compared to the bare GC electrode, which exhibited a smooth and clean surface (Fig. S1†). However, the surface characteristics of the carbon-nanomaterial modified GC electrodes varied with the type of carbon nanomaterials. A 3D nanowire network with hierarchical nanoporous structure (so-called "nano-grass") was found on the CNT/Nafion/GC electrode surfaces (Fig. 1A). However, in the case of the GO/Nafion/GC electrodes, a continuous and dense surface without noticeable nanopores was observed (Fig. 1B). These results could be explained by GO sheet aggregation due to hydrophobicity and interactions. On the other hand, Fig. 1C shows the aggregated carbon nanoparticles, which then formed a 3D and porous surface on the KB/Nafion/GC electrodes (Fig. 1C). All results clearly show the successful modification of the GC electrodes by carbon nanomaterials. All of the electrodes, therefore, were considered suitable for the electrochemical investigation of bioflavonoids.

To further investigate the effects of carbon nanomaterials on the electrocatalysis of bioflavonoids, XRD, Raman spectroscopy and XPS were performed. Fig. 1D shows the XRD patterns of

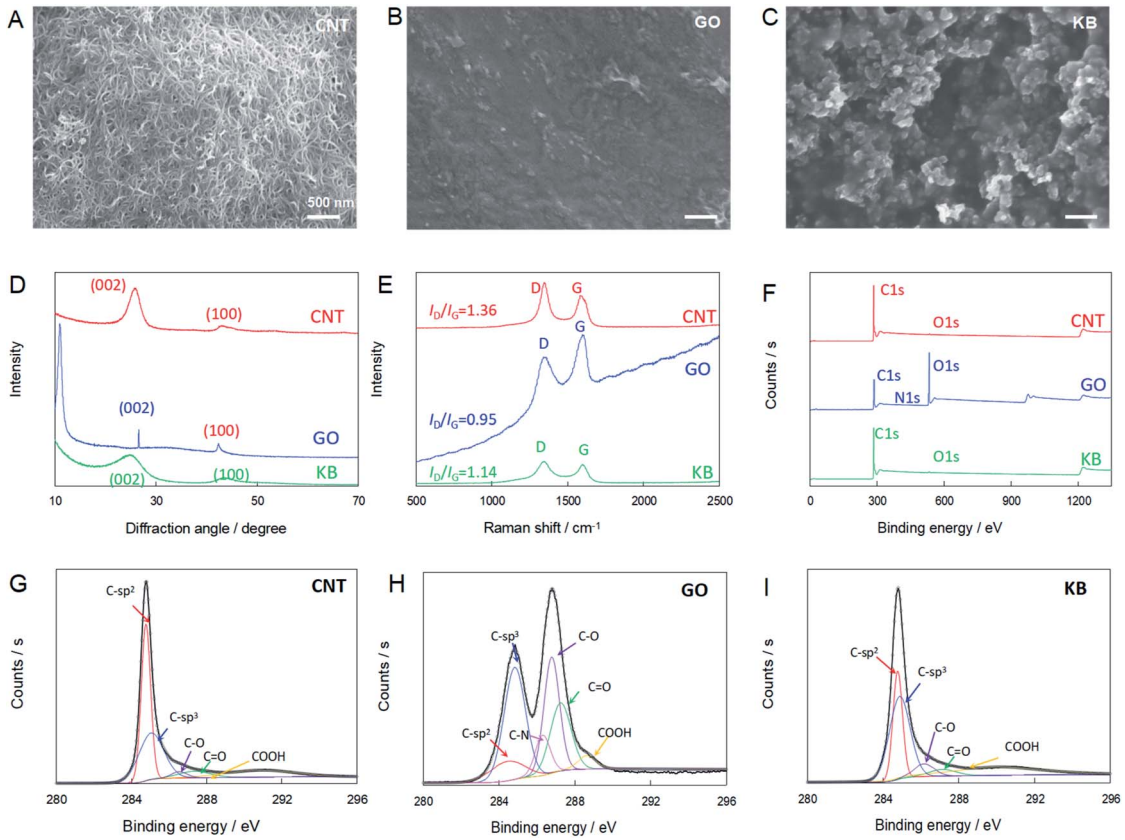

Fig. 1 (A)–(C) SEM images of CNT/Nafion/GC (A), GO/Nafion/GC (B) and KB/Nafion/GC (C). (D) XRD pattern, (E) Raman and (F) XPS survey spectra of CNT, GO and KB. (G)–(I) shows the XPS spectra in C 1s region of CNT, GO and KB.

CNT, GO and KB. Strong diffraction peak at ~25.6° and 43.6°, which corresponded to (002) and (100) crystal faces, indicating the interlayer space in the radial direction and the in-plane graphitic structure of all carbon nanomaterials, respectively. A sharp peak for GO at 11.04° indicated the large interlayer spacing because of the high level oxygen containing groups on graphite lattice.[32]

Raman spectroscopy is a powerful tool for characterizing the structures of carbon nanomaterials. As shown in the Raman spectrum in Fig. 1E, there were two characteristic peaks in all spectra. The first is the D band, which associates with a breathing mode of the *k*-point phonons of the A_{1g} symmetry and is identified at 1344, 1346, and 1346 cm^{-1} for CNT, GO, and KB, respectively. The second peak, the G band, which represents the first-order scattering of the E_{2g} phonon of hexagonal sp^2 carbon atoms, is located at 1584, 1597, and 1595 cm^{-1} for CNT, GO, and KB, respectively. As a result, the ratio between the normalized intensities of the D band and G band, I_D/I_G, which is related to the degree of disorder and defects, was calculated as 1.36, 0.95, and 1.14 for CNT, GO, and KB, respectively. The higher value of I_D/I_G for CNT than for GO and KB indicates more structural defects in the CNTs.[33]

XPS was employed to further evaluate the chemical compositions and carbon bonding states of the three types of carbon nanomaterials. The survey scan spectra of all carbon nanomaterials showed mainly the presence of carbon and oxygen, with trace amounts of Cl, S, and N in GO, which was probably a result of process contamination (Fig. 1F). The percentages of each carbon species relative to the total amount of carbon species were calculated on the basis of the relative surface area of each fitted peak, as shown in Fig. 1G–I and Table S1.† It was found that the concentration of oxygenated carbon species, including C–O, C=O, and COOH was much higher, and that of the sp^2 species was lower, in GO than in CNT and KB. The ratios of sp^2 to sp^3 species for CNT, GO, and KB were 1.25, 0.29, and 0.60, respectively.

Electrocatalysis of bioflavonoids at carbon-nanomaterials modified electrodes

The electrocatalysis of bioflavonoids at the as-prepared carbon-nanomaterial modified GC electrodes was carried out in 0.2 M phosphate buffer solution (pH 7.0 ± 0.1). Fig. 2A shows the cyclic voltammograms (CVs) of the CNT/Nafion/GC electrodes in the absence and presence of bioflavonoids (hesperidin or naringin). No notable redox peak could be detected at the CNT/Nafion/GC electrodes in the entire potential range from 0 to 0.8 V *vs.* Ag|AgCl in phosphate buffer without any bioflavonoids. After the addition of 0.1 mM hesperidin into the electrolyte, an evident anodic peak at *ca.* 0.51 V (P_1) on the forward positive-going scan and two cathodic peaks at *ca.* 0.20 V (P_{2c}) and *ca.* 0.11 V (P_{3c}) on the negative-going scan were observed in the first

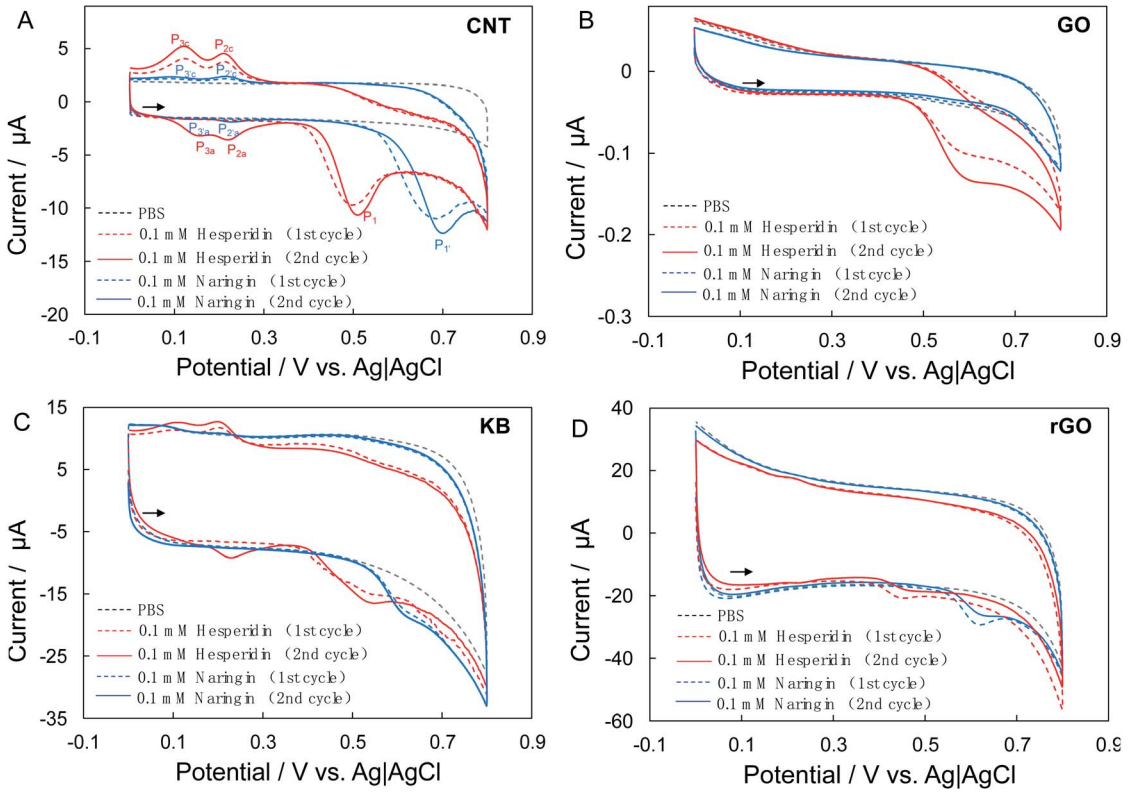

Fig. 2 CVs of CNT/Nafion/GC (A), GO/Nafion/GC (B) and KB/Nafion/GC (C) and rGO/Nafion/GC (D) electrodes in phosphate buffer solutions (pH 7.0 ± 0.1, 0.2 M) in the absence (gray dotted lines) and presence of 0.1 mM hesperidin (red lines) or 0.1 mM Naringin (blue lines) with scan rate of 10 mV s^{-1}. The red and blue broken lines represent the first cycles while solid lines are the second cycles recorded. The arrows show the direction of potential scan.

cycle (Fig. 1A). Furthermore, two new anodic peaks at *ca.* 0.22 V (P_{2a}) and *ca.* 0.14 V (P_{3a}) were recorded on the positive-going scan of the second cycle, followed by the anodic peak (P1) at *ca.* 0.51 V and cathodic peaks at *ca.* 0.20 V (P_{2c}) and *ca.* 0.11 V (P_{3c}). To confirm the sources of these redox peaks, CVs of the CNT/Nafion/GC electrodes with an initial potential of 0.3 V and scan direction of negative were performed. As shown in Fig. S2,† only the anodic peak at *ca.* 0.51 V (P_1) and no redox peak in the range of 0–0.3 V was observed in the first cycle.

Taken together, the anodic peak at *ca.* 0.51 V (P_1), which can be ascribed to the electrooxidation of hesperidin, whereas the redox peak pairs P_{2a}/P_{2c} and P_{3a}/P_{3c} are produced by the oxidation products of hesperidin. Similar behaviors were also found at the CNT/Nafion/GC electrodes in the case of naringin: a clear anodic peak at *ca.* 0.70 V ($P_{1'}$) and two cathodic peaks at *ca.* 0.20 V ($P_{2'c}$)and *ca.* 0.08 V ($P_{3'c}$) during the first cycle. Two new anodic peaks at *ca.* 0.26 V ($P_{2'a}$) and *ca.* 0.11 V ($P_{3'a}$) were found on the second positive-going scan.

Fig. 2B and C show the CVs of the GO/Nafion/GC and KB/Nafion/GC electrodes in the absence and presence of bioflavonoids (hesperidin or naringin). Notable oxidative waves were observed at both the GO/Nafion/GC and KB/Nafion/GC electrodes after the addition of bioflavonoids, although the shapes of the CV curves and the current response to bioflavonoids varied. The electrooxidative waves at the GO/Nafion/GC electrodes showed a residual slope without pronounced peak shapes, indicating the poor electrocatalytic activity of GO toward bioflavonoids. Furthermore, the current responses of the GO/Nafion/GC electrodes to bioflavonoids (both hesperidin and naringin) were smaller than those of the CNT/Nafion/GC and KB/Nafion/GC electrodes.

The surface area of the electrodes does not seem to be the primary factor causing the difference in the electrocatalysis of bioflavonoids. As shown in Fig. 2, the background current (which is roughly related to the electrochemically active surface of the electrodes) of the KB/Nafion/GC electrode is almost three times higher than that of the CNT/Nafion/GC electrode, however, with no noticeable advantages in the current response to bioflavonoids (Fig. 2C).

Considering the characteristic analysis results discussed in above, structural defects, high amounts of C-sp^2 species, and low amounts of oxygenated carbon are seem to play important roles in the electrocatalysis of hesperidin and naringin.[34] To confirm this assumption, a reduced GO(rGO)-modified electrode (rGO/Nafion/GC) was fabricated by the electrochemical reduction of GO/Nafion/GC in phosphate buffer solution (pH 7.0 ± 0.1, 0.2 M) at −1.2 V for 600 s (Fig. S3A†).[35] The obvious increase of I_D/I_G (1.39) indicated the increased structural defects in rGO (Fig. S3B†).[36,37] Consequently, significantly increased background currents and evident peak-shape electrocatalytic waves were detected by the rGO/Nafion/GC electrodes (Fig. 2D).

Kinetic analysis of electrocatalysis of naringin and hesperidin

To further understand the process of electrocatalytic reaction of naringin and hesperidin at CNT/Nafion/GC electrodes, the effects of pH on the peak potentials are investigated. Fig. 4A shows the CVs of CNT/GC electrodes in 0.1 mM hesperidin contained phosphate buffer (0.1 M) with pH from 5.8 to 8.0. It should be noted here that, to clearly show the redox pairs of $P_{2a/2c}$ and $P_{3a/3c}$, the second cycle of CVs are selected. As shown in Fig. 3A, all peaks shift to negative direction with the increase of pH implied that these electrochemical reactions involve proton transfer. Linear relationships between the peak potential and pH value of electrolyte could be found with slopes of −0.058 ($R^2 = 0.998$), −0.059 ($R^2 = 0.998$), −0.055 ($R^2 = 0.998$), −0.057 ($R^2 = 0.992$) an −0.057 ($R^2 = 0.998$) mV pH^{-1} for P_1, P_{2a}, P_{2c}, P_{3a} and P_{3c}, respectively (Fig. 3B). Furthermore, the effect of electrolyte pH on the peak potential of naringin is similar to that of hesperidin: all peaks shift to negative direction with the increase of electrolyte pH (Fig. 3C). Slopes of peak potential–pH plots are −0.060 ($R^2 = 0.997$), −0.059 ($R^2 = 0.997$), −0.060 ($R^2 = 0.998$), 0.061 ($R^2 = 0.997$) and −0.061 ($R^2 = 0.999$) mV pH^{-1} for $P_{1'}$, $P_{2'a}$, $P_{2'c}$, $P_{3'a}$ and $P_{3'c}$, respectively(Fig. 3D). The values of all slopes closed the theoretical value of −59 mV pH^{-1} indicated that electrochemical reactions of hesperidin and naringin occur at CNT/Nafion/GC electrodes with equal number of electrons and protons. Therefore, P_1 (for hesperidin) and $P_{1'}$ (naringin) in Fig. 2A should be ascribed to the electrooxidation reaction of hydroxyl group in ring B, which are one electron-one proton transfer process.[19]

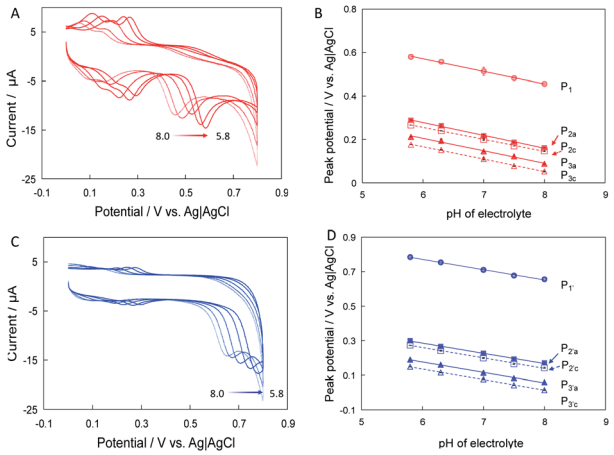

Fig. 3 CVs of CNT/Nafion/GC electrodes in 0.1 mM hesperidin (A) and naringin (C) contained phosphate buffer with pH from 8.0 to 5.8 containing. Relationships between peak potential and pH of electrolytes for hesperidin (B) and naringin (D).

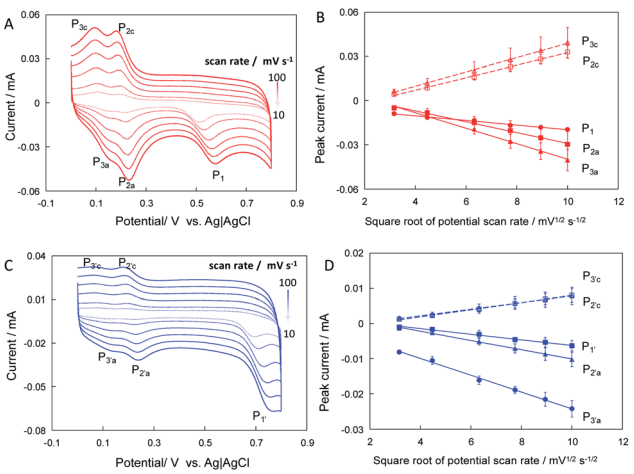

Fig. 4 CVs of CNT/Nafion/GC electrodes in phosphate buffer (pH 7.0 ± 0.1, 0.2 M) containing 0.1 mM hesperidin (A) and naringin (C) with potential scan rate varied from 10 to 100 mV s^{-1}, respectively. Relationships between peak current of CNT/Nafion/GC electrodes and square root of potential scan rate for hesperidin (B) and naringin (D).

Furthermore, the effects of the scan rate on the peak current and peak potentials were examined. Fig. 4A and C show the CVs of CNT/GC electrodes in phosphate buffer containing 0.1 mM hesperidin and naringin at potential scan rates from 10 to 100 mV s^{-1}. All peak currents increased with increasing potential scan rate. The relationships between peak currents and potential scan rates were explored. As shown in Fig. 4B and D, the peak currents of the CNT/Nafion/GC electrodes linearly increased with the square root of the potential scan rate, indicating the diffusion-controlled processes of hesperidin and naringin at the CNT/Nafion/GC electrodes.

Simultaneous detection of hesperidin and naringin in CGT

The high electroactivity of naringin and hesperidin at the CNT/Nafion/GC electrodes makes it suitable for the simultaneous detection of naringin and hesperidin. Fig. 5A–C show the linear scan voltammograms (LSVs) of the CNT modified electrode in the presence of naringin, hesperidin, and mixtures of both with different concentrations. The oxidative currents in all cases increased with the concentration of the substrate, indicating that the current responses are ascribed to the electrooxidation of bioflavonoids. Fig. 5D and E show the relationships between peak current and concentration of hesperidin and naringin, which were added to the electrolyte alone or simultaneously. It can be seen that the current responses in both cases exhibit a similar tendency, indicating no notable interference effects on each other. Finally, the sensitivity of as-prepared CNT/Nafion/GC electrodes to naringin and hesperidin were calculated as 0.15 and 0.11 μA μM^{-1} and with linear ranges of 0–30 μM and 0–40 μM, respectively.

CGT was utilized as a real sample for the simultaneous determination of naringin and hesperidin. The peel of fresh CGT fruits was cut into pieces and directly extracted in methanol using an ultrasonicator for 30 min. After centrifugation, the supernatant was filtered and used for detection. Immediately before each electrochemical measurement, a 10 μL sample solution was transferred into the voltammetric cell containing 10 mL phosphate buffer, and the standard addition method was used to determine the amount of naringin and hesperidin in the CGT extract. Fig. 5G shows the LSVs of the CNT/Nafion/GC electrodes in a phosphate buffer containing CGT extract. The naringin and hesperidin concentrations were calculated using

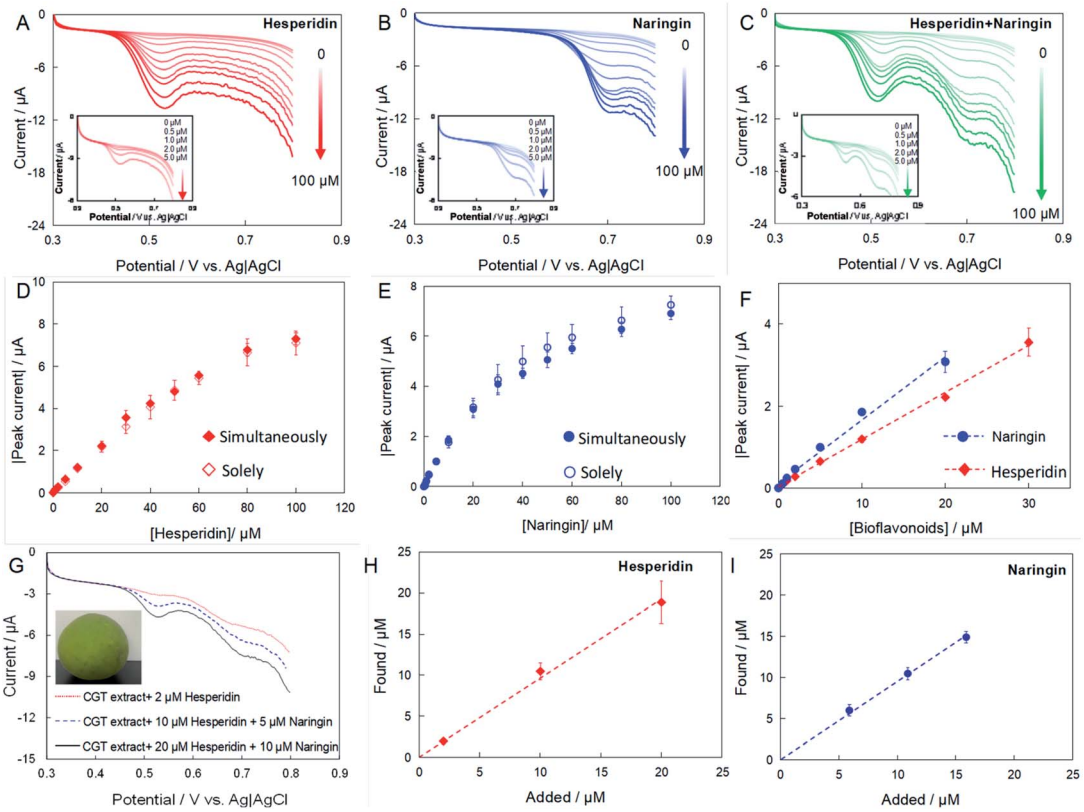

Fig. 5 LSVs of CNT/Nafion/GC electrodes in phosphate buffer with different concentration of hesperidin (A), naringin (B) and mixture of both (C). (D) and (E) show the relationships between peak currents and concentration of bioflavonoids added solely (open symbol) or simultaneously (closed symbol). (F) Calibration curve of hesperidin and naringin. (G) LSV of CNT/Nafion/GC electrodes in phosphate buffer containing CGT extract and different concentration of naringin and hesperidin. (H) and (I) show the relationships between found and added bioflavonoids in phosphate buffer containing CGT extracts.

Table 1 Determination results of naringin and hesperidin in CGT extract

	Detected (by HPLC)/μM		Added/μM		Found/μM		Recovery/%	
Sample name	Naringin	Hesperidin	Naringin	Hesperidin	Naringin	Hesperidin	Naringin	Hesperidin
CGT extracts	5.89 ± 0.05	0.006 ± 0.001	0	2.0	6.0 ± 0.7	2.2 ± 0.1	101.8	109.7
			5.0	10.0	10.5 ± 0.7	11.0 ± 1.0	96.4	109.9
			10.0	20.0	14.9 ± 0.7	19.0 ± 2.0	93.8	99.9

the current response. Fig. 5H and I show the linear relationships between the added concentration and the measured concentration of naringin and hesperidin. The slopes are 0.98 ($R^2 = 0.99$) and 0.95 ($R^2 = 0.99$) for naringin and hesperidin, respectively, indicating the reliability of the as-prepared electrochemical sensors. It is noted here that the original content of naringin and hesperidin in the CGT extract were detected by HPLC and calculated as 5.89 ± 0.01 and 0.006 ± 0.01 μM, respectively. Table 1 shows that the recovery varied from 93.8% to 109.9%, which demonstrates the ability of the CNT/Nafion/GC electrode to simultaneously determine naringin and hesperidin with satisfactory results, and could be employed for practical applications.

Conclusions

In summary, the electrocatalysis of two bioflavonoids at three types of carbon nanomaterial-modified electrodes was investigated and compared. The experimental results show that CNTs, which have more structural defects, higher amounts of C-sp^2, and lower amounts of oxygenated carbon than GO and KB, show excellent catalytic activity for hesperidin and naringin. In contrast, GO showed poor activity for the electrocatalysis of hesperidin and naringin. The poor activity of GO can be improved by the electrochemical reduction of GO. This finding is helpful for studying the electrocatalytic mechanism of bioflavonoids as well as for fabricating electrochemical sensors for bioflavonoid detection. The prepared CNT/Nafion/GC

electrodes were finally utilized for the simultaneous detection of hesperidin and naringin in a CGT extract and showed acceptable sensitivity and high recovery.

Author contributions

HX: conceptualisation, methodology, investigation, writing-original draft/review & editing; TG: methodology, writing–review & editing; RF: methodology, writing–review & editing; JZ: conceptualisation, project administration, writing–review & editing.

Conflicts of interest

There are no conflicts to declare.

Acknowledgements

This work was partially supported by the National Key R&D Program of China (No. 2020YFD1001101); Guangdong Basic and Applied Basic Research Foundation (No. 2019A1515111183); China Agriculture Research System of MOF and MARA; Agricultural Competitive Industry Discipline Team Building Project of Guangdong Academy of Agricultural Sciences (No. 202113TD); Special Fund for Scientific Innovation Strategy-Construction of High Level Academy of Agriculture Science (No. R2020PY-JG001); Scientific Research Foundation for the Introduction of Talent, Guangdong Academy of Agricultural Sciences (No. R2021YJ-YB1001), and President Foundation of Institute of Fruit Tree Research, Guangdong Academy of Agricultural Sciences (No. 202005). The authors also would like to thank Editage (http://www.editage.cn) for English language editing.

References

1 B. Kapoor, M. Gulati, R. Gupta, S. K. Singh, M. Gupta, A. Nabi and P. A. Chawla, *Curr. Org. Chem.*, 2021, **25**, 737–747.
2 P. Karak, *Int. J. Pharma Sci. Res.*, 2019, **10**, 1567–1574.
3 S. J. Maleki, J. F. Crespo and B. Cabanillas, *Food Chem.*, 2019, **29**, 125124.
4 G. C. Jagetia and T. K. Reddy, *Life Sci.*, 2005, **77**, 780–794.
5 P. Bellavite and A. Donzelli, *Antioxidants*, 2020, **9**, 742.
6 F. Meneguzzo, R. Ciriminna, F. Zabini and M. Pagliaro, *Processes*, 2020, **8**, 549.
7 R. Fan, C. Zhu, D. Qiu and J. Zeng, *Int. J. Food Prop.*, 2019, **22**, 1848–1862.
8 C. V. da Silva Padilha, G. A. Miskinis, M. E. A. O. de Souza, G. E. Pereira, D. de Oliveira, M. T. Bordignon-Luiz and M. dos Santos Lima, *Food Chem.*, 2017, **228**, 106–115.
9 Y. Nolvachai and P. J. Marriott, *J. Sep. Sci.*, 2013, **36**, 20–36.
10 L. Mira, M. Tereza Fernandez, M. Santos, R. Rocha, M. Helena Florêncio and K. R. Jennings, *Free Radical Res.*, 2002, **36**, 1199–1208.
11 A. M. Chiorcea-Paquim, T. A. Enache, E. De Souza Gil and A. M. Oliveira-Brett, *Compr. Rev. Food Sci. Food Saf.*, 2020, **19**, 1680–1726.
12 X. Li, R. Zou, Y. Niu, W. Sun, T. Shao and X. Chen, *Sensors*, 2018, **18**, 2309.
13 J. Wang, N. Zhou, Z. Zhu, J. Huang and G. Li, *Anal. Bioanal. Chem.*, 2007, **388**, 1199–1205.
14 J. Tang and B. Jin, *J. Electroanal. Chem.*, 2016, **780**, 46–52.
15 D. Zhang, Y. Zhang and L. He, *Electroanalysis*, 2013, **25**, 2136–2144.
16 P. Kanagavalli, S. Radhakrishnan, G. Pandey, V. Ravichandiran, G. Perumal Pazhani, M. Veerapandian and G. Hegd, *Electroanalysis*, 2020, **32**, 1220–1225.
17 Y. Liao, N. Wang, Y. Ni, J. Xu and S. Shao, *J. Electroanal. Chem.*, 2015, **754**, 94–99.
18 J. Wu, D. Xiao, H. Zhao, H. He, J. Peng, C. Wang, C. Zhang and J. He, *Microchim. Acta*, 2015, **182**, 2299–2306.
19 N. Sebastian, W. C. Yu and D. Balram, *Anal. Chim. Acta*, 2020, **1095**, 71–81.
20 Y. Gao, X. Wu, H. Wang, W. Lu and M. Guo, *Analyst*, 2018, **143**, 297–303.
21 I. V. Zaporotskova, N. P. Boroznina, Y. N. Parkhomenko and L. V. Kozhitov, *Mod. Electron. Mater.*, 2016, **2**, 95–105.
22 M. Pumera, *Electrochem. Commun.*, 2013, **36**, 14–18.
23 H. Inoue, K. Hosoya, N. Kannari and J. I. Ozaki, *J. Power Sources*, 2012, **220**, 173–179.
24 Y. Zhang and Q. Wei, *J. Electroanal. Chem.*, 2016, **781**, 401–409.
25 A. C. Power, B. Gorey, S. Chandra and J. Chapman, *Nanotechnol. Rev.*, 2018, **7**, 19–41.
26 H. Xia and J. Zeng, *Catalysts*, 2020, **10**, 1447.
27 M. Zhang and L. Dai, *Nano Energy*, 2012, **1**, 514–517.
28 M. Zhou, H. L. Wang and S. Guo, *Chem. Soc. Rev.*, 2016, **45**, 1273–1307.
29 H. Xia, Y. Kitazumi, O. Shirai, H. Ozawa, M. Onizuka, T. Komukai and K. Kano, *Bioelectrochemistry*, 2017, **118**, 70–74.
30 Z. Han, L. Zhao, P. Yu, J. Chen, F. Wu and L. Mao, *Electrochem. Commun.*, 2019, **101**, 82–87.
31 R. Fan, Y. Xie, C. Zhu, D. Qiu, J. Zeng and Z. Liu, *Int. J. Biol. Macromol.*, 2019, **138**, 511–518.
32 K. Krishnamoorthy, M. Veerapandian, K. Yun and S. J. Kim, *Annu. Rev. Condens. Matter Phys.*, 2013, **1**, 89–108.
33 M. S. Dresselhaus, A. Jorio and R. Saito, *Annu. Rev. Condens. Matter Phys.*, 2010, **1**, 89–108.
34 S. Šafranko, A. Stanković, A. Asserghine, M. Jakovljević, S. Hajra, S. Nundy, M. Medvidović-Kosanović and S. Jokić, *Electroanalysis*, 2021, **33**, 1063–1071.
35 K. Q. Deng, J. H. Zhou and X. F. Li, *Colloids Surf., B*, 2013, **101**, 183–188.
36 S. Y. Toh, K. S. Loh, S. K. Kamarudin and W. R. W. Daud, *Chem. Eng. J.*, 2014, **251**, 422–434.
37 Y. Xu, M. Gao, G. Zhang, X. Wang, J. Li, S. Wang and Y. Sang, *Chin. J. Catal.*, 2015, **36**, 1936–1942.